Chinese Chemical Letters 33 (2022) 1047–1050

Contents lists available at ScienceDirect

Chinese Chemical Letters

journal homepage: www.elsevier.com/locate/cclet

Co-POM@MOF-derivatives with trace cobalt content for highly efficient oxygen reduction

Yitao Song[a], Yewang Peng[a], Shuang Yao[a,*], Peng Zhang[a], Yujie Wang[a], Jianmin Gu[b,*], Tongbu Lu[a], Zhiming Zhang[a,*]

[a] Institute for New Energy Materials and Low Carbon Technologies,School of Materials Science & Engineering, School of Chemistry and Chemical Engineering, Tianjin University of Technology, Tianjin 300384, China
[b] State Key Laboratory of Metastable Materials Science and Technology (MMST), Yanshan University, Qinhuangdao 066004, China

ARTICLE INFO

Article history:
Received 28 June 2021
Revised 19 July 2021
Accepted 8 August 2021
Available online 12 August 2021

Keywords:
Metal-organic framework
Polyoxometalate
Polyoxoanion
Oxygen reduction
Electrocatalysis

ABSTRACT

A simple and effective method for constructing highly efficient oxygen reduction catalysts with trace amount of isolated cobalt was firstly developed by the pyrolysis of Co-centered polyoxometalate@metal-organic framework (Co-POM@MOF). The Co-centered polyoxometalate ($[CoW_{12}O_{40}]^{6-}$) was confined in the well-defined void space of ZIF-8 to achieve homogeneous dispersion of polyoxoanions, where the isolated Co centers were well surrounded by the W-O shell and ZIF-8 framework. The Co-POM@MOF-derived N-doping porous carbon (Co-W-NC) with trace cobalt content was facilely prepared by the pyrolysis of the Co-POM@MOF under Ar atmosphere. The single dispersion of polyoxoanions in the metal-organic framework with complete separation of Co center surrounding by W-O shell and ZIF-8 framework ensures the uniform dispersion of Co atoms, confirmed by the Fourier transform extended X-ray absorption fine structure measurement. The Co-W-NC composite catalysts exhibit high performance for oxygen reduction reactions with a half-wave potential of 0.835 V in 0.1 mol/L KOH solution with excellent durability, which is much superior to that of the control samples derived from the $[PW_{12}O_{40}]$@ZIF-8, and the commercial Pt/C. This work highlights a new insight for constructing highly efficient catalysts *via* the introduction of metal-centered polyoxometalate into metal-organic framework following the high temperature treatment process.

Proton exchange membrane batteries and metal-air batteries have the advantages of sufficient energy conversion efficiency, low emissions, high energy density, which are of great significance in energy storage and chemical production. However, due to the complex paths and slow kinetics, their performance was seriously influenced by the oxygen reduction reactions (ORRs) at the cathodes. At present, platinum-based precious catalysts were usually explored to drive the ORR [1-3]. Due to the low reserves of the expensive Pt, its commercial application has been significantly restricted, and the development of low-cost and efficient catalysts is of great significance to promote the commercial application of fuel cells. In recent years, non-noble metal ORR catalysts such as metal oxides [4,5], nitrides [6,7] and phosphides [8,9] have shown great potential, and in this research field a series of Fe-based single atom catalysts have been developed to drive the ORR [10-15].

Polyoxometalates (POMs) are a typical class of molecular clusters with nanometer size, structure and composition diversity, it has attracted widespread attention in the field of magnetism, optics and catalysis [16-22]. However, the limited specific surface area of POM itself has limited its application in catalysis. Therefore, more and more efforts have been denoted to disperse POM in the porous materials to enhance their catalytic performance [23-30]. In this filed, various POMs have been encapsulated into the metal-organic framework (MOF) matrix to achieve the uniform dispersion of polyoxoanions, which can be used as efficient catalysts for efficient water splitting, CO_2 reduction, and organic synthesis [31-35]. ZIFs, as a typical class of the MOFs, have suitable pore size and structure, which has become a suitable single-atom carrier in recent years *via* the pyrolysis of the metal-doping MOFs [36-40]. Encapsulation of POM into the ZIF framework has been achieved to construct POM@MOF functional material [41-43], which can be used as the precursor to construct high-performance catalyst *via* the pyrolysis process by replacing doping metal with POM clusters [44,45].

* Corresponding authors.
E-mail addresses: shuangyao@email.tjut.edu.cn (S. Yao), jmgu@ysu.edu.cn (J. Gu), zmzhang@email.tjut.edu.cn (Z. Zhang).

https://doi.org/10.1016/j.cclet.2021.08.045
1001-8417/

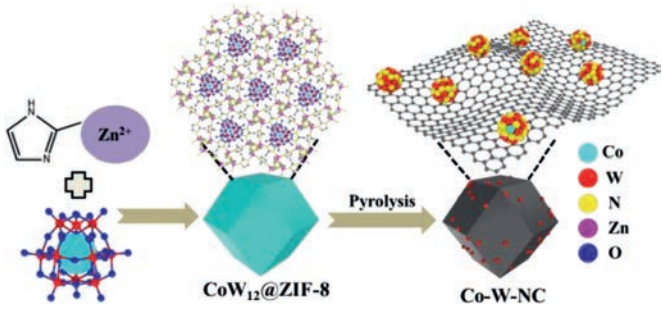

Fig. 1. Schematic show of the synthetic procedure of Co-W-NC.

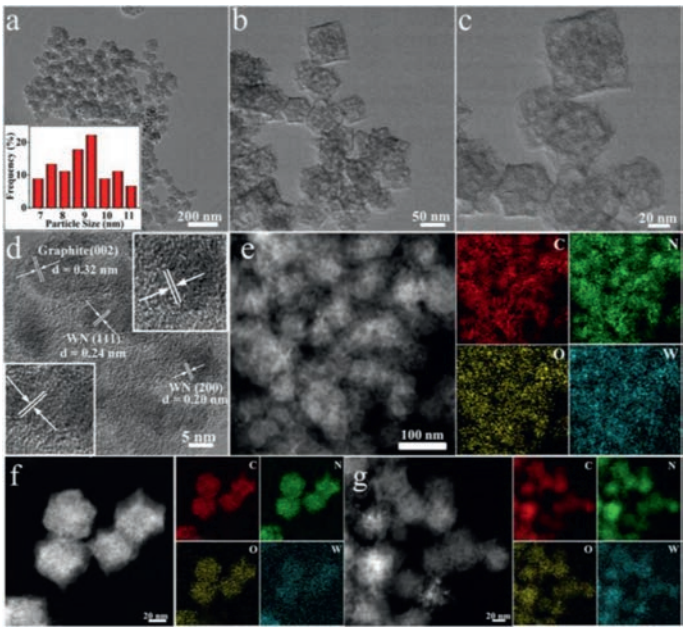

Fig. 2. (a-c) TEM images of Co-W-NC. (d) HRTEM images of Co-W-NC showing the existence of WN in the Co-W-NC. (e) EDS elemental mapping images of Co-W-NC. EDS elemental mapping images of CoW_{12}@ZIF-8 after different temperatures: (f) 825 °C, (g) 875 °C.

In the past decades, transition metal-substituted POMs have been widely developed and used as efficient catalysts for various reactions [46-48]. The transition metal centers can be encapsulated into POM to realize the effective isolation of central metal from the POM shell. Further, the POM is dispersed in MOF matrix to further isolate the polyoxoanion, the double isolation effect will help prevent the agglomeration of transition metal centers during the pyrolysis process to build single-atom catalysts. Based on this idea, Co-centered POM of $[CoW_{12}O_{40}]^{6-}$ ($[CoW_{12}]$) was *in situ* encapsulated into the cavity of ZIF-8 to construct a CoW_{12}@ZIF-8 host-guest composite. After high temperature pyrolysis, a highly dispersed Co-W-NC material doped with trace amount of cobalt centers was obtained. The single dispersion of polyoxoanions in the MOF matrix with complete separation of Co center surrounding by W-O shell ensures the uniform dispersion of Co atoms to expose more active sites, thereby ensuring that the trace amount of Co has excellent ORR activity. The Co-W-NC catalysts exhibit excellent ORR performance with a half-wave potential of 0.835 V in 0.1 mol/L KOH solution, which is much better than the control sample derived from the isostructural $[PW_{12}O_{40}]^{3-}$ ($[PW_{12}]$) anion, where P center was used to replace the Co center in the POMs. The durability test shows that Co-doping composite catalyst exhibits excellent chemical stability during the electrocatalytic process.

The Co-W-NC was synthesized *via* a two-step strategy (Fig. 1), where the $[CoW_{12}]$ anion was first encapsulated into the molecular cages *via in situ* synthesis of ZIF-8 to construct POM@ZIF-8 composite. As shown in Fig. S1 (Supporting information), the CoW_{12}@ZIF-8 composite shows a polyhedral morphology, similar to that of the isolated ZIF-8 reported in the literatures [49]. Fourier Transform Infrared (FTIR) spectra of CoW_{12}@ZIF-8 was found to have extra peaks as well as shifted peaks in comparison to that of isolated POM and ZIF-8, respectively. As shown in Fig. S2 (Supporting information), the characteristic peaks of ZIF-8 are more prominent in the FT-IR spectrum of CoW_{12}@ZIF-8. For the POM, a strong peak at 1620 cm^{-1} makes the reversed intensity of two peaks near 1585 cm^{-1} and 1637 cm^{-1} in the FT-IR spectrum of composite.

Moreover, a new peak appears at ~874 cm^{-1} in the FT-IR spectrum CoW_{12}@ZIF-8, matching with that of POM anion. A slight shift was observed as the interactions between POM surface and interior sites of ZIF-8. These results together with the PXRD confirm the formation of the CoW_{12}@ZIF-8 composite. The thermogravimetric analysis (TGA) shows that the residual mass of CoW_{12}@ZIF-8 at 900°C is 22.62%, much higher than that of isolated ZIF-8, indicating the introduction of POMs into the MOF matrix (Fig. S3 in Supporting information). Then, the resulting CoW_{12}@ZIF-8 composite was pyrolysis under the Ar atmosphere to synthesize the Co-W-NC material doped with trace amount of cobalt centers. The morphology of Co-W-NC was characterized by scanning electron microscopy (SEM) and transmission electron microscopy (TEM). As shown in Figs. 2a-c and Fig. S4 (Supporting information), Co-W-NC has relatively uniform rhombic dodecahedral morphology, similar to that of the CoW_{12}@ZIF-8. The particle sizes are in the range of 50-100 nm. The CoW_{12}@ZIF-8 calcined at 825 °C and 875 °C have similar morphologies to those of Co-W-NC (Fig. S5 in Supporting information). HR-TEM shows that there are evenly distributed nanoparticles on the carbon substrate with the sizes in the range of 6-12 nm. The lattice spacing of 0.20 nm and 0.24 nm corresponds to the (200) and (111) crystal plane of WN, respectively (Fig. 2d) [50,51]. Elemental mapping images showed that C, N, O and W elements were distributed homogenously throughout the entire architecture (Figs. 2e-g). However, no Co-based particles can be observed in the HR-TEM images. These results were consistent with that of PXRD results, where the peaks of WN can be detected obviously, however no diffraction peaks related to the Co-based nanoparticles can be observed. Accordingly, $[CoW_{12}]$ in the cavity transferred into the WN and isolated cobalt centers during the pyrolysis treatment, as the aggregation of Co centers can be well prevented by the separated cavity in ZIF-8 and the W-O shell.

PXRD measurement proves the successful synthesis of $[CoW_{12}]$ and the composite of $[CoW_{12}]$@ZIF-8 (Figs. S6a and b in Supporting information), which ensures the encapsulation of $[CoW_{12}]$ without altering the structure of ZIF-8. As shown in Fig. 3a, after calcination, both the peaks of in the PXRD of $[CoW_{12}]$ and ZIF-8 disappeared. Several sharp diffraction peaks at 37.4°, 43.8°, 63.7° and 76.4° appeared, which match well with the (111), (200), (220) and (311) planes of WN (JCPDS No. 75-1012), indicating the complete decomposition of the MOF structure and formation of WN nanoparticles. X-ray photoelectron spectroscopy (XPS) was then used to characterize the surface composition of the catalyst. The C 1s spectrum shows two peaks at 284.8 and 285.5eV of to C-C and C-O (Fig. S7a in Supporting information), and the high resolution N 1s spectrum of all the samples confirmed the presence of pyridinic N (398.8 eV), pyrrolic N (401.0 eV), and graphitic N (402.2 eV) in the Co-W-NC samples (Fig. 3b). As shown in Fig. 3c, the binding energies at 35.7 and 37.8 eV were obviously detected in the W 4f spectrum, which can be attributed to W $4f_{7/2}$ and W $4f_{5/2}$ of respectively [52,53]. This result indicated that the formation of WN element into the NC *via* the pyrolysis of the POM@MOF composite,

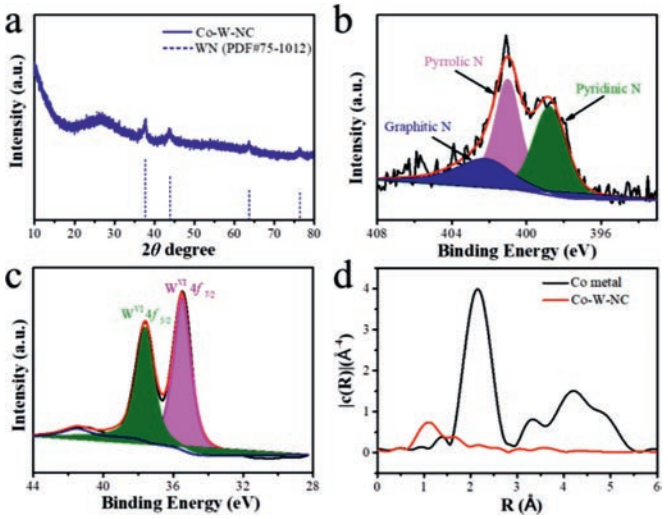

Fig. 3. (a) XRD patterns of Co-W-NC. (b) N 1s XPS spectra of Co-W-NC. (c) W 4f XPS spectra of Co-W-NC. (d) FT-EXAFS curves of Co-W-NC.

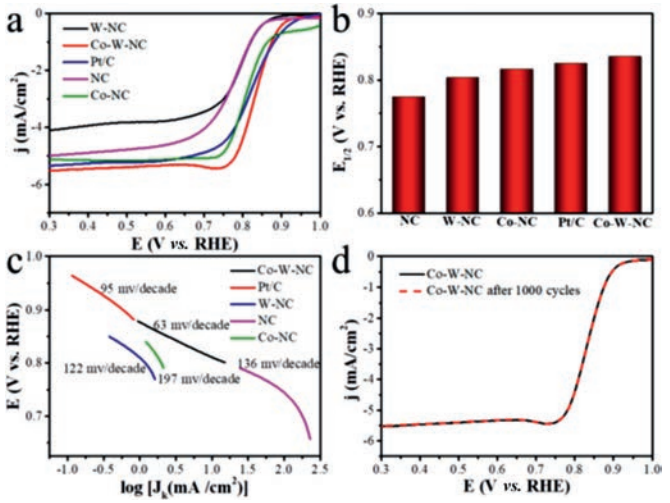

Fig. 4. (a) Polarization curves for Co-W-NC and the references. (b) The contrast between Co-W-NC and the references for $E_{1/2}$. (c) Tafel slopes of Co-W-NC and the references. (d) The long-term durability tests of Co-W-NC.

which was further confirmed by the ICP-MS result (3.7%). We also tried to determine the Co element in the Co-W-NC sample. However, no obvious Co XPS signal can be detected, indicating a trace amount of Co centers in the Co-W-NC sample (Fig. S7b in Supporting information). To verify this speculation, ICP-MS measurement was performed to determine the Co content, where a maximum Co content was determined to be lower than 0.1%. According to the formula of $[CoW_{12}O_{40}]^{6-}$, where the quality ratio of Co/W can be determined to be 2.67/100, the maximum content of Co can be easily calculated to be 0.098%, which was consistent with that of the ICP-MS result. As a result, only trace amount was introduced into the Co-W-NC sample, so there were no obvious signals of Co in the XPS and X-ray absorption near-edge spectroscopy (XANES) (Fig. 3d). However, in the FT-EXAFS curve, a Co-N or Co-C bonding can be observed, however no obvious Co-Co bond can be detected. This result reveals the single atom dispersion of the Co centers in the NC, as the aggregation of isolated cobalt atoms can be well prevented by both the separated cavity in ZIF-8 and the W-O shell. We also attempt to determine the single-atom dispersion of Co centers by atomic-resolution high angle annular dark-field scanning TEM imaging. However, it is not possible as the ultra-small element number of Co (59) compared with that of W (183). To confirm the important role of the trace amount Co centers in the POM@MOF–derived porous NC, the isostructural $[PW_{12}O_{40}]$ anion, where P center was used to replace the Co center in the POMs was used to synthesize the $[PW_{12}O_{40}]$@ZIF composite to further construct W-NC sample, where related measurement of the IR spectra confirm the presence of the $[PW_{12}O_{40}]$ (Fig. S8 in Supporting information).

The ORR activity of Co-W-NC and all the control samples was investigated in O_2-saturated 0.1 mol/L KOH aqueous solution with rotating disk electrode (RDE), Ag/AgCl and graphite rod as the working, reference and counter electrode, respectively. To assess the ORR activity, the cyclic voltammetry (CV) curves of Co-W-NC was examined in N_2 and O_2 saturated 0.1 mol/L KOH aqueous solution. As depicted in Fig. S9 (Supporting information), an obvious cathodic peak was detected in the O_2-saturated electrolyte, however, no obvious reduction peak was found in the N_2-saturated solution, predicting its effective electrocatalytic ORR activity. Fig. 4a shows the polarization curves of all the samples and commercial 20% Pt/C with a positively shifting order: Co-W-NC > Pt/C > Co-NC > W-NC > NC. Especially, the Co-W-NC displayed an optimal activity with the highest half-wave potential of 0.835 V, much higher than that of $[CoW_{12}]$@ZIF-8 calcined at 825 °C and 875 °C (Fig. S10 in Supporting information), and the NC ($E_{1/2}$ = 0.774 V) derived from the isolated ZIF-8. As a result, the sample of Co-W-NC showed excellent oxygen reduction performance, and its oxygen reduction activity was far better than that of 20% commercial Pt/C.

In order to prove the important role of encapsulation of $[CoW_{12}O_{40}]^{6-}$ into ZIF-8 to construct Co-doping NC, a series of control samples were synthesized to perform the ORR experiments. Firstly, we added an equivalent amount of Co^{2+} ($Co(NO_3)_2{\cdot}6H_2O$) cations instead of $[CoW_{12}O_{40}]^{6-}$ in the synthesis of ZIF-8 to construct the Co-NC. As shown in Fig. 4b, its ORR performance was much lower than that of the Co-W-NC. Further, an isostructural Keggin-type POM $[PW_{12}O_{40}]$ with a P atom replacing the Co center in the $[CoW_{12}O_{40}]^{6-}$ anion was encapsulated into the ZIF-8 MOF to synthesize the PW_{12}@ZIF-8, which was confirmed by the IR characterizations. The obtained composite PW_{12}@ZIF-8 was further used to synthesize the W-NC *via* a similar pyrolysis treatment process to that of the Co-W-NC. As shown in Fig. 4b, the oxygen reduction test reveals that the W-NCs exhibits a much lower $E_{1/2}$ potential of 0.803 V for ORR compared to that of Co-NC, especially for Co-W-NC (0.835 V). These results indicate that the Co single atom can serve as the active sites for ORR, and the Co-W-NC obtained by the Co-POM@MOF strategy is far superior to Co-NC ($E_{1/2}$ = 0.816 V) and the W-NC for the ORR.

The specific activity-potential relationship was further evaluated *via* the Tafel plots. Co-W-NC possesses a Tafel slope of 63 mV/dec, significantly lower than that of other samples (Fig. 4c). This indicates that Co-W-NC may undergo a faster dynamics during the ORR. Moreover, the Co-W-NC has a lower electrochemical reaction resistance compared to the other samples as revealed by electrochemical impedance spectroscopy (EIS) measurements, suggesting the enhanced electron transport and fast kinetic process for Co-W-NC (Fig. S11 in Supporting information). In addition to ORR activity, the Co-W-NC exhibits an excellent cycling stability, which can retain its initial activity even after 1000 catalytic cycles (Fig. 4d). To further assess electron transfer number (n), ORR is performed for Co-W-NC by altering the rotation speed of rotating disk electrode (RDE) (Figs. S12a and b in Supporting information). As calculated according to Koutecky-Levich (K-L) equation, when the Co-W-NC with a loading of 0.5 mg/cm^2, n is calculated to be

4.1 at different potentials, suggesting a four electron process and first-order reaction kinetics.

In summary, we developed simple and effective method for synthesizing highly efficient oxygen reduction catalysts with trace amount of isolated cobalt atoms by the pyrolysis of Co-POM@MOF. The Co-POM $[CoW_{12}O_{40}]^{6-}$ was confined in the well-defined void space of the ZIF-8 MOF to achieve the homogeneous dispersion of polyoxoanions in the MOF matrix, where the Co single atom centers were well surrounded by the W-O shell and the ZIF-framework. The POM@MOF-derived composite Co-W-NC exhibits highly efficient ORR activity. Systematic experiments revealed that trace amount of Co centers played important role in constructing the ORR catalyst, and its ORR activity was much superior to that of the control sample derived from the $[PW_{12}O_{40}]$@ZIF-8 composite, and the commercial 20% Pt/C with excellent stability. This method provides a new avenue for the synthesis of Co single atom, and it can be used as a substitute for Pt/C catalysts for practical application.

Declaration of competing interest

The authors declare that they have no known competing financial interests or personal relationships that could have appeared to influence the work reported in this paper.

Acknowledgment

This work was supported by the Natural Science Foundation of Tianjin City of China (No. 18JCJQJC47700).

Supplementary materials

Supplementary material associated with this article can be found, in the online version, at doi:10.1016/j.cclet.2021.08.045.

References

[1] Z.X. Song, Y.N. Zhu, H.S. Liu, et al., Small 16 (2020) e2003096.
[2] J. Liu, J. Bak, J. Roh, et al., ACS. Catal. 11 (2020) 466–475.
[3] J. Liu, M.G. Jiao, B.B. Mei, et al., Angew. Chem. Int. Ed. 58 (2019) 1163–1167.
[4] G.P. Wu, J. Wang, W. Ding, et al., Angew. Chem. Int. Ed. 55 (2016) 1340–1344.
[5] R.J. Wu, M. Liu, Y.W. Peng, et al., Chin. Chem. Lett. 30 (2019) 989–994.
[6] X.L. Tian, J.M. Luo, H.X. Nan, et al., J. Mater. Chem. A 3 (2015) 16801–16809.
[7] Y. Yuan, J.C. Wang, S. Adimi, et al., Nat. Mater. 19 (2020) 282–286.
[8] H.T. Liu, J.Y. Guan, S.X. Yang, et al., Adv. Mater. 32 (2020) e2003649.
[9] M. Li, T.T. Liu, X.J. Bo, et al., Nano Energy 33 (2017) 221–228.
[10] Y. Mun, S. Lee, K. Kim, et al., J. Am. Chem. Soc. 141 (2019) 6254–6262.
[11] Y. Lei, F.W. Yang, H.M. Xie, et al., J. Mater. Chem. A 8 (2020) 20629–20636.
[12] W. Ye, S.M. Chen, Y. Lin, et al., Chem 5 (2019) 2865–2878.
[13] Y. Wang, D. Wang, Y. Li, Smart Mater. 2 (2021) 56–75.
[14] J.Z. Li, H.G. Zhang, W. Samarakoon, et al., Angew. Chem. Int. Ed. 58 (2019) 18971–18980.
[15] S Li, B. Li, L. Ma, J. Yang, H.X. Xu, Chin. Chem. Lett. 28 (2017) 2159–2163.
[16] H.L. Wu, Z.M. Zhang, Y.G. Li, X.L. Wang, E.B. Wang, CrystEngComm 17 (2015) 6261–6268.
[17] Z.J. Liu, X.L. Wang, C. Qin, et al., Coord. Chem. Rev. 313 (2016) 94–110.
[18] S.S. Wang, G.Y. Yang, Chem. Rev. 115 (2015) 4893–4962.
[19] L.Z. Qiao, M. Song, A.F. Geng, S. Yao, Chin. Chem. Lett. 30 (2019) 1273–1276.
[20] P.T. Ma, F. Hu, J.P. Wang, J.Y. Niu, Coord. Chem. Rev. 378 (2019) 281–309.
[21] N. Li, J. Liu, B.X. Dong, Y.Q. Lan, Angew. Chem. Int. Ed. 59 (2020) 20779–20793.
[22] X.B. Han, Z.M. Zhang, T. Zhang, et al., J. Am. Chem. Soc. 136 (2014) 5359–5366.
[23] T. He, X.B. Xu, B. Ni, et al., Angew. Chem. Int. Ed. 57 (2018) 10148–10152.
[24] S. Zhang, X. Wang, H.X. Zhang, Z.H. Zhao, X.L. Wang, Chin. Chem. Lett. 29 (2018) 309–312.
[25] Z.M. Zhang, T. Zhang, C. Wang, et al., J. Am. Chem. Soc. 137 (2015) 3197–3200.
[26] N. Zhang, L. Hong, A. Geng, et al., Chin. Chem. Lett. 29 (2018) 1409–1412.
[27] Y.J. Wang, Y.Y. Zhou, H.G. Hao, et al., Inorg. Chem. 57 (2018) 1342–1349.
[28] H. Li, S. Yao, H.L. Wu, et al., Appl. Catal. B 224 (2018) 46–52.
[29] A.X. Yan, S. Yao, Y.G. Li, et al., Chem. Eur. J. 20 (2014) 6927–6933.
[30] H. Wang, Y.P. Chen, Z.C. You, M.X. Zhou, N. Zhang, Chin. Chem. Lett. 26 (2015) 187–192.
[31] Q.X. Han, C. He, M. Zhao, et al., J. Am. Chem. Soc. 135 (2013) 10186–10189.
[32] L.J. Zhang, T.Q. Mi, M.A. Ziaee, et al., J. Mater. Chem. A 6 (2018) 1639–1647.
[33] Y.R. Wang, Q. Huang, C.T. He, et al., Nat. Commun. 9 (2018) 4466.
[34] A.M. Zhang, M. Zhang, D. Lan, et al., Inorg. Chem. 57 (2018) 11726–11731.
[35] X.J. Kong, Z.K. Lin, Z.M. Zhang, T. Zhang, W.B. Lin, Angew. Chem. Int. Ed. 55 (2016) 6411–6416.
[36] D. Liu, J.C. Li, S. Ding, et al., Small 4 (2020) 1900827.
[37] B.S. Liu, H. Zhou, H.H Jin, et al., Chin. Chem. Lett. 32 (2021) 535–538.
[38] M.L. Xiao, H. Zhang, Y.T. Chen, et al., Nano Energy 46 (2018) 396–403.
[39] T. Sun, L. Xu, D. Wang, Y. Li, Nano Res. 12 (2019) 2067–2080.
[40] C.X. Zhao, B.Q. Li, J.N. Liu, Q. Zhang, Chin. Chem. Lett. 30 (2019) 911–914.
[41] R. Li, X.Q. Ren, J.S. Zhao, et al., J. Mater. Chem. A 2 (2014) 2168–2173.
[42] M. Samaniyan, M. Mirzaei, R. Khajavian, H. Eshtiagh-Hosseini, C. Streb, ACS Catal. 9 (2019) 10174–10191.
[43] V.K. Abdelkader-Fernández, D.M. Fernandes, S.S. Balula, L. Cunha-Silva, C. Freire, ACS Appl. Energy Mater. 3 (2020) 2925–2934.
[44] Q. Lan, Z.M. Zhang, C. Qin, et al., Chem. Eur. J. 22 (2016) 15513–15520.
[45] Y.Y. Ma, C.X. Wu, X.J. Feng, et al., Energy Environ. Sci. 10 (2017) 788–798.
[46] Q. Lan, S.J. Jin, Z.M. Zhang, Chin. Sci. Bull. 63 (2018) 3286–3295.
[47] Q. Lan, Z.M. Zhang, Y.G. Li, Y. Lu, E.B. Wang, Dalton Trans. 43 (2014) 16265–16269.
[48] S. Wang, Y.W. Liu, Z. Zhang, et al., ACS Appl. Mater. Interfaces 11 (2019) 12786–12796.
[49] S. Mukhopadhyay, J. Debgupta, C. Singh, A. Kar, S.K. Das, Angew. Chem. Int. Ed. 57 (2018) 1918–1923.
[50] Y.L. Wang, T. Nie, Y.H. Li, et al., Angew. Chem. Int. Ed. 56 (2017) 7430–7434.
[51] C. Lv, X.B. Wang, L.J. Gao, et al., ACS. Catal. 10 (2020) 13323–13333.
[52] B. Zhang, J.G. Hou, Y.Z. Wu, et al., Adv. Energy. Mater. 9 (2019) 1803693.
[53] J.Q. Yan, L.Q. Kong, Y.J. Ji, et al., Nat. Commun. 10 (2019) 2149.